JOURNAL OF COMPUTATIONAL PHYSICS 117, 79–89 (1995)

Adaptive Singularity Method for Stokes Flow Past Particles

HUA ZHOU AND C. POZRIKIDIS

Department of Applied Mechanics & Engineering Sciences, 0411, University of California at San Diego, La Jolla, California 92093-0411

Received March 15, 1994; revised September 1, 1994

We implement the method of fundamental solutions to compute Stokes flow past or due to the motion of solid particles. The flow is represented in terms of a collection of vectorial fundamental solutions to the governing equations including the point force, the potential dipole, and the couplet. The locations and strengths of the fundamental solutions are computed by minimizing a functional so as to satisfy the required boundary conditions with highest accuracy. The method is applied to compute flow past or due to the motion of spherical and spheroidal particles in an infinite fluid and in a semi-infinite fluid bounded by a plane wall. The computed locations and strengths of the singularities are compared with those corresponding to exact discrete and continuous singularity representations, and the computed force and torque exerted on the particles are compared with exact values available from analytical solutions. It is found that the method yields excellent accuracy with a moderate number of singularities in an extended range of particle aspect ratios up to ten, and for ratios of the particle center to wall separation h and particle radius a as low as $h/a = 1.05$. The computed singularity solutions are used to establish generalized Faxen laws for the force and torque.

1. INTRODUCTION

The method of fundamental solutions, or singularity method, has found extensive applications in computing solutions to a broad range of problems involving elliptic partial differential equations in the fields of electromagnetics, acoustic scattering, potential flow, Stokes flow, and elastostatics. The basic idea is to express the solution in terms of a collection of singular fundamental solutions to the governing equations, located outside the domain of solution, and then compute the strength and possibly the location of the fundamental solutions in order to satisfy the boundary conditions in some optimal sense.

In the present work we consider Stokes flow past stationary or moving rigid particles. Although exact singularity representations are available for a limited number of cases involving infinite flow past or due to the motion of particles with spherical and ellipsoidal shapes [1–5], the existence of exact representations for more general shapes and types of flow has not been established. The derivation of approximate singularity representations, however, is motivated by successful computation and supportive theoretical evidence [6, 7]. Furthermore, the application of singularity methods may be justified on the basis of the boundary integral representation, by observing that the latter provides us with a solution in terms of a continuous boundary distribution of Green's functions and their derivatives. One might expect that condensing the distributed singularities into discrete points and moving their poles outside the domain of flow will not have a critical effect on the structure of the flow even in the vicinity of the boundaries.

Apart from providing us with approximate solutions for given boundary conditions, the singularity representation of the flow due to the motion of a rigid particle and of the disturbance flow due to presence of a particle in a linear flow has the added benefit that it provides us with the generalized Faxen relations [5]. The latter yield the force and torque exerted on a particle as well as the associated coefficient of the stresslet when the particle is held stationary in an arbitrary incident flow, in terms of the values of the incident velocity and its derivatives at the location of the singularities inside the particle. Evaluation of the force is prerequisite for computing particle trajectories in a viscous fluid, whereas evaluation of the coefficient of the stresslet is necessary for computing the effective stress tensor of dilute suspensions.

Recent developments in the area of generalized boundary integral methods for Stokes flow have raised the importance of accurate singularity representations. In the compound boundary integral method, the flow due to a particle that is held stationary in an incident flow is represented in terms of a collection of singularities including point forces and couplets and a complementary component that is expressed in terms of a double-layer hydrodynamic potential [4, 5]. The advantage of this dual representation is that the mathematical problem is reduced to solving a well-posed integral equation of the second kind, which may be done using efficient iterative methods. Having available an accurate singularity representation expedites the solution of the integral equation and therefore reduces the cost of the computations.

The majority of computational studies of Stokes flow past particles using the method of fundamental solutions have been conducted by introducing a collection of singularities at fixed locations inside the particle and then by computing the strengths of the singularities so as to satisfy the boundary conditions in some approximate sense [4]. Recent work, however, has shown that substantial gain in accuracy may be achieved by relaxing

0021-9991/95 $6.00

the restriction that the singularities are located at fixed positions and by computing the optimal location of the singularities simultaneously with their strengths. Allowing the singularities to move as a part of an optimization problem in connection with an elliptic partial differential equation was first proposed by Mathon and Johnston [8]. The method was subsequently applied with success to study a number of problems in the fields of electromagnetics, potential flow, heat transport, elastostatics, Stokes flow in cavities, and acoustic scattering due to an obstacle in a fluid or a solid [9–16]. Karageorghis and Fairweather [17–20], in particular, solved a series of problems governed by Laplace's or the biharmonic equation, and Karageorghis [21] obtained numerical solutions to free boundary problems governed by Laplace's equation.

Our main objective in the present paper is to investigate the performance of the adaptive singularity method for problems of external Stokes flow. In Section 2 we outline the principles of the method and discuss the numerical implementation. One noteworthy feature of the present formulation is that the fundamental solutions are selected a priori so as to satisfy the boundary conditions of vanishing normal and tangential velocity on the boundaries the flow, thereby simplifying the computations. In the present implementation, the fundamental solutions are computed in terms of derivatives of Green's functions. Furthermore, the types of fundamental solutions are selected according to the physical requirement that the force and torque exerted on a particle have finite values independently of the number of singularities involved in the approximate representation.

In the first part of the numerical study we compare the optimal singularity representations that emerge from solving an optimization problem to the exact discrete or continuous representations available for particles with spherical and spheroidal shapes. Apart from demonstrating the accuracy and limitations of the method, these comparisons address the question of whether the converged locations and strengths of the numerical representations may provide evidence for the existence of exact representations, as well as illustrate the type of the exact representations.

In the second part of the numerical study we examine the performance of the method for problems of a semi-infinite flow bounded by a plane wall. Overall, the results suggest that satisfactory accuracy can be achieved with moderate computational effort, even for quite small particle-to-wall separation, and this corroborates the application of the method by itself or in combination with a boundary integral method to more general problems of particulate flow.

Computation of the flow past or due to the motion of a particle in term of singularities in low- and high-Reynolds number flows is enjoying increasing popularity, and the derivation of accurate singularity representations will enhance the physical relevance of dynamical simulations based on discrete models [22]. The present work suggests that a substantial gain in accuracy may be obtained by straightforward modifications of the basic implementation involving singularities with fixed poles.

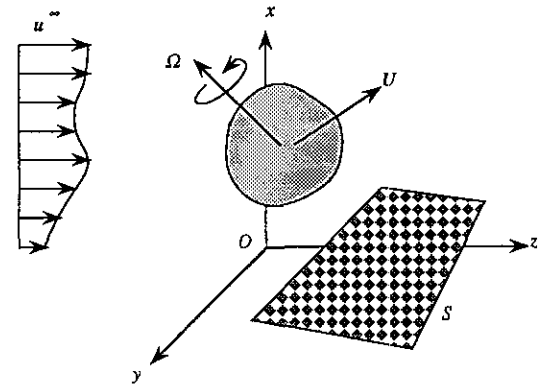

FIG. 1. Schematic illustration of Stokes flow past, or due to the translation and rotation of a solid particle in the presence of a boundary.

2. METHOD FORMULATION AND IMPLEMENTATION

Consider a three-dimensional Stokes flow $\mathbf{u}^\infty$ past a rigid particle, or flow due to the translation and rotation of a rigid particle, as illustrated in Fig. 1. The motion of the fluid is governed by the continuity equation and the stokes equation for the velocity $\mathbf{u}$ and pressure P,

$$\nabla \cdot \mathbf{u} = 0, \quad -\nabla P + \mu \nabla^2 \mathbf{u} = 0, \tag{1}$$

where μ is the viscosity of the fluid. If the particle translates with velocity $\mathbf{U}$ and rotates with angular velocity Ω about a selected center $\mathbf{X}$, the no-slip and no-penetration conditions require that on the surface the particle $\mathbf{u} = \mathbf{U} + \Omega \times (\mathbf{x} - \mathbf{X})$. In the case of flow in an infinite domain, the disturbance flow due to the particle must decay far from the particle. In all cases, the velocity is required to vanish over any stationary solid boundary S.

To describe the flow due to the particle we introduce a representation in terms of a collection of fundamental solutions or singularities of the governing equations (1). These include the Green's function, representing the flow due to a point force, the point source, and other derivative singularities discussed in reference [5]. In the present implementation, we use two-index singularities denoted by $S_{ij}^{(n)}$, with strengths $q_j^{(n)}$ and poles $\mathbf{x}^{(n)}$ located within the particle, including the point force, the couplet, and the point source dipole, thus writing

$$v_i(\mathbf{x}) = u_i^\infty(\mathbf{x}) + \sum_{n=1}^{N} S_{ij}^{(n)}(\mathbf{x}, \mathbf{x}^{(n)}) q_j^{(n)}, \tag{2}$$

where $\mathbf{v}$ is an approximation to the exact flow $\mathbf{u}$. The singularities are designed so as to satisfy the boundary conditions over S, that is, $S_{ij}^{(n)}(\mathbf{x}, \mathbf{x}^{(n)}) = 0$ when $\mathbf{x}$ is on S. The specific form

of the singularities for flow in an infinite domain and in a semi-infinite domain bounded by a plane wall can be found in [5] and, in the interest of space, will not be repeated. The stress field corresponding to the flow (2) is given by

$$\sigma_{ik}(\mathbf{x}) = \sigma^{\infty}_{ik}(\mathbf{x}) + \sum_{n=1}^{N} T^{(n)}_{ijk}(\mathbf{x}, \mathbf{x}^{(n)}) q^{(n)}_j, \tag{3}$$

where $\mathbf{T}^{(n)}$ is the stress tensor corresponding to the fundamental solutions [5].

It can be shown that, with the exception of the point source, all the fundamental solutions of Stokes flow may be expressed in terms of derivatives of the Green's function $\mathbf{G}$ representing the flow due to a point force. Thus, the representation (2) may be written in the equivalent form

$$v_i(\mathbf{x}) = u^{\infty}_i(\mathbf{x}) + \sum_{n=1}^{N} L^{(n)}_{kj} \langle G_{ij}(\mathbf{x}, \mathbf{x}^{(n)}) \rangle q^{(n)}_k, \tag{4}$$

where the operators $\mathbf{L}^{(n)}$, acting with respect to $\mathbf{x}^{(n)}$, determine the nature of the fundamental solutions. For instance, in the case of the point force $\mathbf{L}$ is the identity operator $\mathbf{I}$, in the case of the point source dipole $\mathbf{L} = (-\frac{1}{2})\mathbf{I}\nabla^2$, and in the case of the couplet $L_{kj} = (\frac{1}{2})\varepsilon_{klj}\, \partial/x_l$.

For flow due to a particle that translates or rotates in an otherwise quiescent fluid, we exploit the linearity of the solution on the velocity of translation $\mathbf{U}$ and angular velocity of rotation Ω to write, respectively,

$$\begin{aligned} v_i(\mathbf{x}) &= U_k \sum_{n=1}^{N} M^{(n)}_{kj} \langle G_{ij}(\mathbf{x}, \mathbf{x}^{(n)}) \rangle, \\ v_i(\mathbf{x}) &= \Omega_k \sum_{n=1}^{N} N^{(n)}_{kj} \langle G_{ij}(\mathbf{x}, \mathbf{x}^{(n)}) \rangle, \end{aligned} \tag{5}$$

where $\mathbf{M}$ and $\mathbf{N}$ are operators that determine the nature and distribution of the fundamental solutions and are linear combinations of the fundamental operators $\mathbf{L}^{(n)}$. The generalized Faxen relations provide us with the force $\mathbf{F}$ and torque $\mathbf{T}$ on a stationary particle that is immersed in an ambient flow in the form [5]

$$F_k = 8\pi\mu \sum_{n=1}^{N} M^{(n)}_{kj} \langle u^{\infty}_j \rangle, \quad T_k(x) = 8\pi\mu \sum_{n=1}^{N} N^{(n)}_{kj} \langle u^{\infty}_j \rangle. \tag{6}$$

The approximate singularity representations provide us with an approximation to the operators $\mathbf{M}$ and $\mathbf{N}$ involved in (6).

2.1. *Computation of the Singularity Representation*

Mathon and Johnston [8] proposed computing the strengths and locations of the singularities so as to satisfy the boundary conditions with the highest possible accuracy. This is done by minimizing an appropriate functional G which is typically derived by performing the Galerkin or least-squares projection on the boundary conditions.

To derive an appropriate functional for Stokes flow in the presence of a particle, we introduce the Lorentz reciprocal theorem stating that any two flows $\mathbf{u}^{(1)}$ and $\mathbf{u}^{(2)}$ that vanish at infinity with corresponding boundary tractions $\mathbf{f}^{(1)}$ and $\mathbf{f}^{(2)}$, must satisfy the reciprocal relation

$$\int_B \mathbf{u}^{(1)} \cdot \mathbf{f}^{(2)}\, dS = \int_B \mathbf{u}^{(2)} \cdot \mathbf{f}^{(1)}\, dS, \tag{7}$$

where $\mathbf{f} = \sigma \cdot \mathbf{n}$, σ is the stress tensor, and $\mathbf{n}$ is the unit vector normal to the particle surface pointing into the ambient fluid [5]. Applying (7) with $\mathbf{u}^{(1)} = \mathbf{u} - \mathbf{u}^{\infty}$ and $\mathbf{u}^{(2)} = \mathbf{v} - \mathbf{u}$ and requiring the boundary condition $\mathbf{u} = \mathbf{U} + \Omega \times (\mathbf{x} - \mathbf{X})$, we obtain

$$\begin{aligned} \mathbf{U} \cdot \Delta\mathbf{F} + \Omega \cdot \Delta\mathbf{T} = &\int_B [\mathbf{v} - \mathbf{U} - \Omega \times (\mathbf{x} - \mathbf{X})] \cdot \mathbf{f}^{(1)}\, dS \\ &+ \int_B \mathbf{u}^{\infty} \cdot \mathbf{f}^{(2)}\, dS, \end{aligned} \tag{8}$$

where Δ indicates the error due to the approximations involved in the singularity representation (2).

In the absence of an incident flow the second integral on the right-hand side of (8) vanishes and, in order to compute the force $\mathbf{F}$ and torque $\mathbf{T}$ exerted on the particle with highest accuracy, we must minimize the functional represented by the first integral on the right-hand side. Approximating the tractions due to the flow $\mathbf{u}$ with those due to the flow $\mathbf{v}$, we interpret this integral as the projection of the error in the required boundary conditions onto the traction field associated with the singularity representation (2).

In practice, to reduce the cost associated with the computation of the boundary tractions, we prefer to use the alternative least-squares functional

$$G \equiv \int_B |\mathbf{v} - \mathbf{U} - \Omega \times (\mathbf{x} - \mathbf{X})|^2\, dS \tag{9}$$

which has been the standard choice in previous studies [9–21]. Minimizing G with respect to the strength of the singularities yields a system of linear algebraic equations for $\mathbf{q}^{(n)}$, whereas minimizing it with respect to the location of the singularities yields a nonlinear algebraic system for $\mathbf{x}^{(n)}$. Previous computations solved the problem using standard minimization methods but, since the number of fundamental solutions we employ is moderate, we prefer to use standard Newton's iterations.

The iterations proceed by first guessing the optimal position $\mathbf{x}^{(n)}$ of each fundamental solution, solving the linear system of equations for the optimal strength of the singularities $\mathbf{q}^{(n)}$, and then solving the nonlinear system of equations for the new positions of the singularities while maintaining the strengths fixed. Thus, to initialize the computation, we supply the initial

locations of the singularities but not their strengths. The Jacobian matrix for Newton's iterations is computed analytically in simple cases and numerically for the more involved cases. The global iterations are terminated when the difference in both the strength and position of the singularities between the current and previous step is less than a threshold value which is typically set to 10^{-6}.

To reduce the computational cost even further, we replace the differential surface element dS in (9) over the surface of spheres or spheroids with the product $d\xi d\eta$, where ξ and η are the natural surface spheroidal coördinates. We use the 128-point 15th-degree spherical product Gauss quadrature for integration over a spherical particle [23], and the 4-point Gauss quadrature in both the azimuthal and polar coördinates for integration over properly defined boundary elements over a spheroidal particle. The computations were carried out on a SUN SPARCstation 1, and require from less than 1 min to 10 min of CPU time in each case.

3. EXACT REPRESENTATIONS

To investigate the performance of the numerical method, we consider flow in an infinite domain and compare the numerical results with available exact, discrete or continuous, singularity solutions.

3.1. *Sphere*

The flow due to a sphere of radius a that translates with velocity $\mathbf{U}$ may be represented exactly in terms of a Stokeslet, denoted as G_{ij}, and a potential dipole, denoted as D_{ij}, both placed at the center of the sphere as

$$u_i(\mathbf{x}) = \tfrac{3}{4}aU_jG_{ij}(\mathbf{x}, \mathbf{x}^c) - \tfrac{1}{4}a^3U_jD_{ij}(\mathbf{x}, \mathbf{x}^c), \qquad (10)$$

where $\mathbf{x}^c$ is the instantaneous position of the center of the sphere which, for convenience, is placed at the origin [5]. Using the numerical method with a Stokeslet and a potential dipole allowed to move along the axis of translation alone, we recover the exact solution within a few iterations for a wide range of initial guesses. For instance, when the singularities are placed initially at $x^G/a = 0.5$ and $x^D/a = -0.4$ the computations converge in three iterations, whereas when $x^G/a = 0.95$ and $x^D/a = -0.9$ the iterations converge in five iterations. When the initial location of the singularities is too close to the surface, however, the numerical method converges to a local minimum that is different from the global minimum corresponding to the exact solution. This occurs, for instance, when both singularities are placed initially at $x/a = 0.99$, in which case the converged values are respectively $x^G/a = 0.992$ and $x^D/a = -0.984$.

Similar behaviors occur when the singularities are allowed to move in three dimensions. For instance, when the initial guess for the Stokeslet is $\mathbf{x}^G/a = (0.2, 0.4, -0.3)$ and for the potential dipole $\mathbf{x}^D/a = (-0.1, -0.3, 0.2)$, we recover the exact solution in two iterations. When $\mathbf{x}^G/a = (0.8, 0, 0)$ and $\mathbf{x}^D/a = (-0.7, 0, 0)$, on the other hand, the singularities converge to $\mathbf{x}^G/a = (0.974076, 0, 0)$ and $\mathbf{x}^D/a = (-0.709524, 0, 0)$ with corresponding strengths scaled respectively by aU and a^3U, equal to $(0.562, 0, 0)$ and $(-0.000470, 0, 0)$.

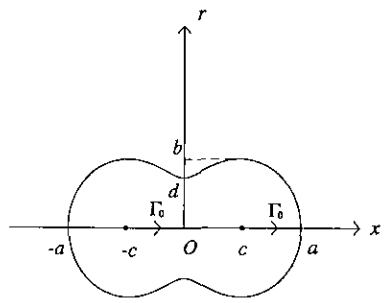

FIG. 2. The flow due to the axial rotation of dumbbell-shaped bodies may be represented by a pair of isolated couplets placed at the focal points.

The flow due to a sphere that rotates with angular velocity Ω may be represented exactly in terms of a single couplet C_{ij} as

$$u_i(\mathbf{x}) = a^3\Omega_jC_{ij}(\mathbf{x}, \mathbf{x}^c) \qquad (11)$$

[5]. Applying the numerical method with a single couplet yields the exact solution within a few iterations. For instance, when the initial position of the couplet is at $x/a = 0.99$, the couplet moves and sits on the center of the sphere in six iterations.

3.2. *Dumbbell-Shaped Bodies*

Chwang and Wu [1] showed that the velocity field due to a class of dumbbell-shaped bodies rotating around their axis with angular velocity Ω may be represented exactly in terms of a pair of couplets with equal strengths Γ_0 located at the focal points of the dumbbells as illustrated in Fig. 2. The azimuthal component of the velocity is

$$u_\theta = \frac{\Gamma_0}{2}\left\{\frac{r}{[(x-c)^2 + r^2]^{3/2}} + \frac{r}{[(x+c)^2 + r^2]^{3/2}}\right\}$$
$$\Gamma_0 = \Omega(c^2 + d^2)^{3/2} = \Omega\frac{(a^2 - c^2)^3}{a(a^2 + 3c^2)}. \qquad (12)$$

The three geometrical parameters a, c, and d are defined in Fig. 2. Our computations with two couplets symmetrically situated and allowed to move along the x axis, converged to the exact solution within a few iterations. If the couplets are placed initially too close to the center of the dumbbell, the iterations converge to a local minimum with the couplets collapsed at $x = 0$. In the other extreme case where the couplets are placed initially too close to the surface of the dumbbell, for instance at $x/a = \pm 0.99$, the solution converges to a local minimum with the couplets located almost on the surface of the dumbbells.

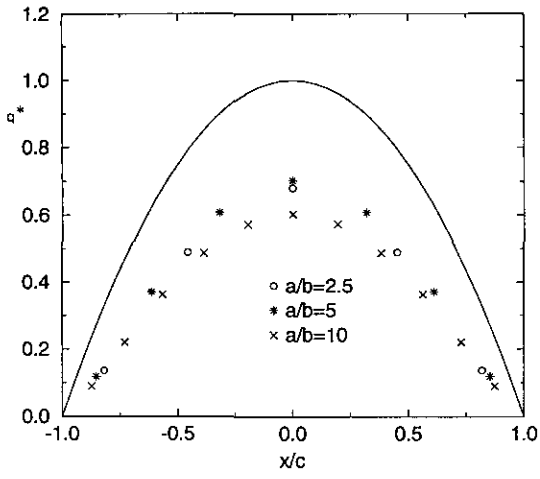

FIG. 3. Computed strengths of couplets for a prolate spheroid with aspect ratio $a/b = 2.5$, 5, and 10, rotating around its major axis. The parabola indicates the continuous distribution corresponding to the exact solution.

3.3. *Rotating Prolate Spheroids*

We consider next a case in which the exact singularity representation takes the form of a continuous distribution. Chwang and Wu [1] showed that the flow produced by a prolate spheroid that rotates about its major axis with angular velocity Ω may be represented in terms of a continuous distribution of couplets over the focal length of the spheroid with parabolic density as

$$u_i = \Omega \Big/ \left[\frac{2e}{1-e^2} - \ln\left(\frac{1+e}{1-e}\right) \right] \int_{-c}^{c} (c^2 - x_0^2) C_{il}(\mathbf{x}, \mathbf{x}_0)\, dx_0, \tag{13}$$

where e is the eccentricity of the spheroid defined as $e = c/a$, $0 < e < 1$, where c is the focal length of the spheroid given by $c^2 = a^2 - b^2$, and a and b are the major and minor axes of the spheroid.

In the numerical method we represent the flow using a set of N couplets oriented along the x axis and distributed evenly and symmetrically over the focal length of the spheroid. The couplets are allowed to move during the iterations but only along the axis of rotation. The results show that for a spheroid with a small aspect ratio $a/b = 2.5$, five couplets are sufficient to yield the torque exerted on the spheroid accurate to the third significant figure. In the converged solution, the position of the couplets are $x^{(n)}/(ab)^{1/2} = 0, \pm 0.658951, \pm 1.188660$ and the computed torque coefficient $\lambda = T/[\mu\Omega(ab)^{3/2}]$ is equal to 0.487374, while the exact value is 0.487524. The strengths of the singularities are distributed in a nearly parabolic manner in agreement with the exact solution as shown in Fig. 3, where $q^* = q/[\Omega(ab)^{3/2}]$. If the exact representation were unknown, this behavior would indicate the existence of an exact singularity representation with parabolic density distribution.

For a spheroid with a higher aspect ratio, a larger but still moderate number of singularities is required to achieve satisfactory accuracy. For instance, when $a/b = 5$, using seven couplets yields $\lambda = 0.312993$ which is lower by less than 1% from the exact value 0.315769. The converged locations of the singularities are $x^{(n)}/(ab)^{1/2} = 0, \pm 0.697557, \pm 1.341298$, and ± 1.871404. The distribution of the corresponding strengths shown in Fig. 3 exhibits a parabolic shape in accord with the exact solution. For a spheroid with $a/b = 10$, using nine couplets yields $\lambda = 0.202172$ which differs from the exact value 0.215184 by about 6%. The converged locations of the singularities are $x^{(n)}/(ab)^{1/2} = 0, \pm 0.691743, \pm 1.364495, \pm 1.998701$, and ± 2.574553. The accuracy is substantially improved by including more couplets. For instance, using 11 couplets we obtain $\lambda = 0.208492$ which differs from the exact value by 3.1%. The corresponding distribution of the dimensionalized strengths of the couplets $q^* = q/[\Omega(ab)^{3/2}]$ is shown in Fig. 3. These results indicate that the discrete singularity representation is effective for elongated but not too slender bodies.

3.4. *Translating Prolate Spheroids*

Chwang and Wu [2] showed that the flow produced by a prolate spheroid that translates with velocity $\mathbf{U}$ may be represented in terms of a distribution of Stokeslets $\mathbf{G}$ and potential dipoles $\mathbf{D}$, over the focal length of the spheroid, oriented in the direction of translation, with constant and parabolic densities, respectively, in the form

$$u_i = U_k A_{kj} \Big/ \left[\left(\frac{2e}{1-e^2}\right) - \ln\left(\frac{1+e}{1-e}\right) \right] \int_{-c}^{c} \left[G_{ij}(\mathbf{x}, \mathbf{x}_0) - \left(\frac{1-e^2}{2e^2}\right)(c^2 - x_0^2) D_{ij}(\mathbf{x}, \mathbf{x}_0) \right] dx_0, \tag{14}$$

where $\mathbf{A}$ is a diagonal matrix with

$$A_{11} = e^2 \Big/ \left[-2e + (1+e^2) \ln\left(\frac{1+e}{1-e}\right) \right],$$
$$A_{22} = A_{33} = -2e^2 \Big/ \left[-2e + (1-3e^2) \ln\left(\frac{1+e}{1-e}\right) \right]. \tag{15}$$

First, we consider axisymmetric motion along the x axis. For a spheroid with moderate aspect ratio, $a/b = 2.5$, we obtain accurate solutions with three Stokeslets and three potential dipoles symmetrically distributed, allowed to move, and oriented along the x axis. The computed drag force coefficient $\lambda = D/[\mu U(ab)^{1/2}] = 0.619061$ agrees with the exact value 0.619039 in the fourth significant figure. The converged positions of the Stokeslets are $x^G/(ab)^{1/2} = 0, \pm 1.093752$ and the corresponding strengths are $q^G/[U(ab)^{1/2}] = 0.352954$ and 0.133053. For the dipoles we obtain $x^D/(ab)^{1/2} = 0, \pm 1.043479$ and $q^D/[U(ab)^{3/2}] = -0.020467, -0.006499$. When the aspect

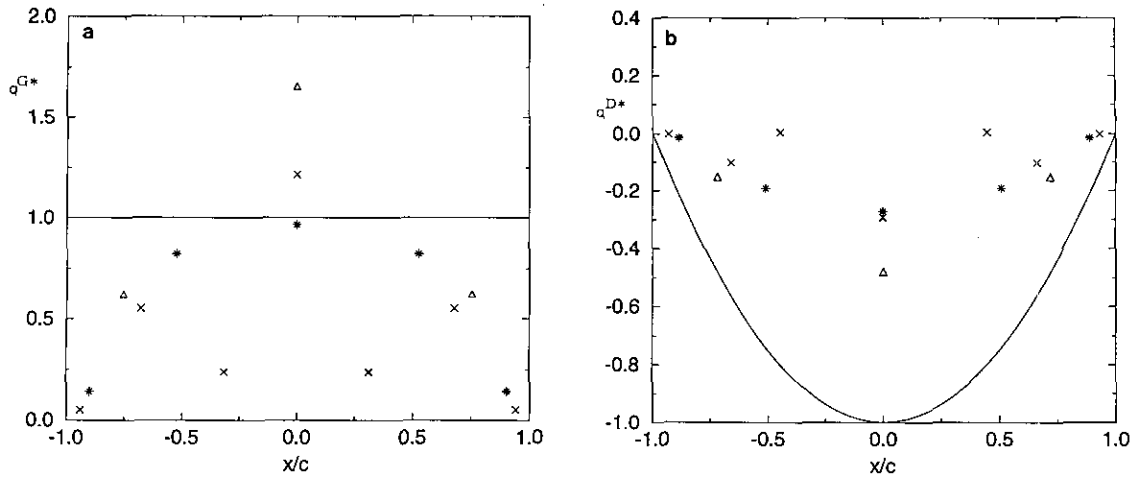

FIG. 4. Strengths of (a) the Stokeslets, and (b) the potential dipoles over the focal length of a spheroid with aspect ratio $a/b = 2.5$ translating along its major axis, computed using 3, 5, and 7 singularities. The forms of the exact continuous distributions are indicated with solid lines.

ratio is increased to $a/b = 5$, five Stokeslets and five potential dipoles are needed to achieve a comparable accuracy. The computed reduced drag coefficient $\lambda = 0.598676$ agrees with the exact value 0.598643 in the fourth significant figure. In the converged solution, the Stokeslets are located at $x^G/(ab)^{1/2} = 0$, ± 1.262965, and ± 2.004412 and their strengths are $q^G/[U(ab)^{1/2}] = 0.192127$, 0.149278, and 0.053997. The potential dipoles are located at $x^D/(ab)^{1/2} = 0$, ± 1.212363, and ± 1.964228 and their strengths are $q^D/[U(ab)^{3/2}] = -0.004280$, -0.002921, and -0.000584. Results for large aspect ratios are also remarkably accurate. For $a/b = 10$, seven Stokeslets and seven potential dipoles yield $\lambda = 0.627844$ which agrees with the exact value 0.627823 in the fourth significant figure. For $a/b = 15$, the same number of singularities results in a less than 0.13% difference in the computed drag coefficient $\lambda = 0.663730$ and the exact value 0.664767.

In Figs. 4a, b we plot the distribution of the reduced strengths of the Stokeslets $q^{G*} = q^G/[U(ab)^{1/2}]$ and potential dipoles $q^{D*} = q^D/[U(ab)^{3/2}]$ over the focal length of the spheroid for $a/b = 2.5$, varying the number of singularities. The distribution of the strengths of the Stokeslets shows significant deviations from the exact uniform profile, whereas the distribution of the strengths of the dipoles exhibits a nearly parabolic shape. In both cases, we observe oscillatory behavior when the number of singularities is increased to seven. If the exact solution were not known, the approximate singularity representation would not be able to indicate it in an unambiguous manner, although, curiously enough, it produces the force and torque with remarkable accuracy.

The performance of the numerical method in the case of transverse translation is comparable to that for axial motion at moderate aspect ratios. For instance, for a spheroid with

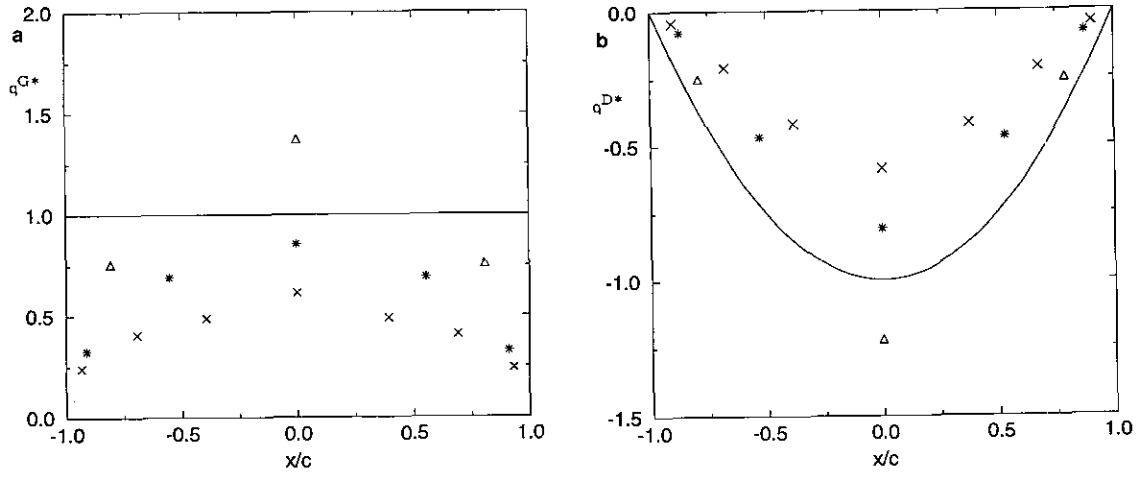

FIG. 5. Strengths of (a) the Stokeslets, and (b) the potential dipoles over the focal length of a spheroid with $a/b = 2.5$ translating along its minor axis, computed using 3, 5, and 7 singularities. The forms of the exact continuous distributions are indicated with solid lines.

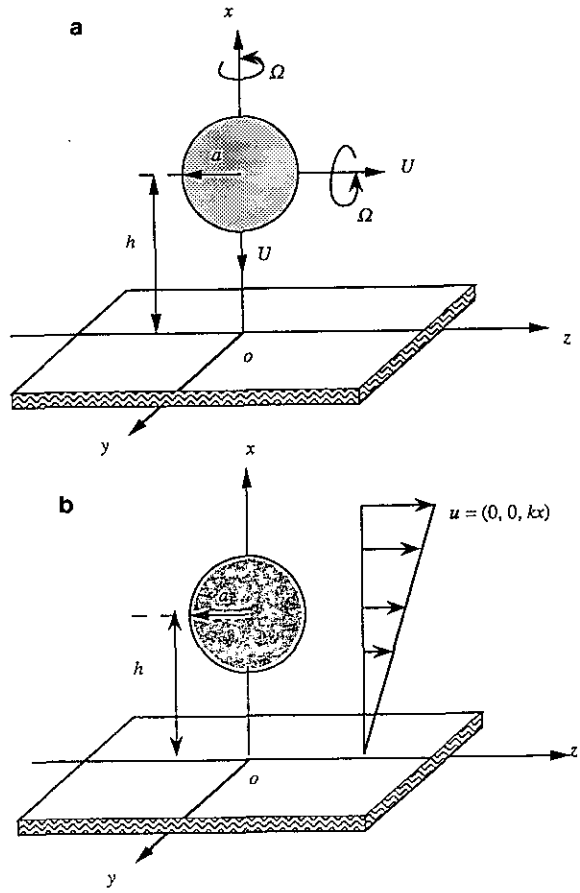

FIG. 6. Illustration of (a) flow due to the translation and rotation of a solid spherical particle in a semi-infinite domain bounded by a plane wall; (b) flow past a stationary sphere placed in a semi-infinite simple shear flow above a plane wall.

$a/b = 2.5$, we obtain accurate solutions with five Stokeslets and five potential dipoles that are free to move along the major axis, distributed symmetrically and oriented in the direction of translation. The computed drag force coefficient $\lambda = 0.73811$ agrees with the exact value 0.73818 in the fourth significant figure. In the converged solution, the Stokeslets are located at $x^G/(ab)^{1/2} = 0, \pm 0.802937$, and ± 1.322621 and their strengths are $q^G/[U(ab)^{1/2}] = 0.218584$, 0.176082, and 0.083683. The potential dipoles converge at $x^D/(ab)^{1/2} = 0, \pm 0.76674$, and ± 1.26805 with strengths $q^D/[U(ab)^{3/2}] = -0.041016$, -0.023784, and -0.004043. The behavior of the distributions of the strengths of the Stokeslets and potential dipoles for $a/b = 2.5$ are shown in Figs. 5a, b. As the number of singularities is increased the distributions tend to the constant or parabolic distributions required by the exact solution. Curiously, the performance of the method for transverse motion, with an associated three-dimensional flow, is better than that for axial motion with an associated axisymmetric flow.

For a moderate aspect ratio $a/b = 5$, using seven Stokeslets and seven potential dipoles yields $\lambda = 0.795162$ which agrees with the exact value 0.795246 in the third significant figure. In the converged solution we obtain $x^G/(ab)^{1/2} = 0, \pm 0.887398$, ± 1.600411, and ± 2.071695 with $q^D/[U(ab)^{1/2}] = 0.173924$, 0.143795, 0.109205, and 0.057621 for the Stokeslets and $x^D/(ab)^{1/2} = 0, \pm 0.884838, \pm 1.586815$, and ± 2.054529 with $q^D/[U(ab)^{3/2}] = -0.016184, -0.010643, -0.004600$, and -0.000675 for the potential dipoles. Computations with a higher number of singularities failed to converge, thus placing limits on the capability of the numerical method. Furthermore, accurate solutions could not be obtained for higher aspect ratios. Computations with a relatively small number of singularities provided unsatisfactory accuracy, whereas those with a large number of singularities failed to converge.

4. A SPHERE IN SEMI-INFINITE FLOW BOUNDED BY A PLANE WALL

In the second part of the numerical study we consider the flow due to the motion or presence of a spherical particle above a plane wall and compare the numerical results with known analytical solutions in bipolar coördinates [4, 24]. In the numerical method we use fundamental solutions that satisfy the condition of vanishing velocity over the wall, derived in terms of the corresponding Green's function of Stokes flow [5].

4.1. *Sphere Translating along or Rotating around an Axis Normal to the Wall*

We begin by considering axisymmetric flow due to a sphere of radius a translating perpendicular to the plane wall along the x axis as shown in Fig. 6a and represent the flow in terms of a point force and a potential dipole located, oriented, and allowed to move along the x axis. In Figs. 7a, b we plot the converged displacement of the position of the point force and potential dipole from the center of the sphere $\delta = (x - h)/a$, as a function of the sphere-to-wall separation h/a, and the corresponding dimensionless strength of the singularities $q^{G*} = q^G/(Ua)$ and $q^{D*} = q^D/(Ua^3)$. As the sphere approaches the wall, both singularities move off the center of the sphere

TABLE I

Drag Coefficient λ for a Sphere Moving Toward a Plane Wall

h/a	Present method	Exact solution	Fixed singularity location
∞	1	1	1
10.067662	1.125245	1.1252465	1.125156
6.1322895	1.221980	1.2219882	1.221223
3.7621957	1.412795	1.4128629	1.405933
2.3524096	1.836388	1.8374749	1.770373
1.5430806	3.007633	3.0360641	2.385381
1.1276260	7.056133	9.2517663	2.927308
1	∞	∞	∞

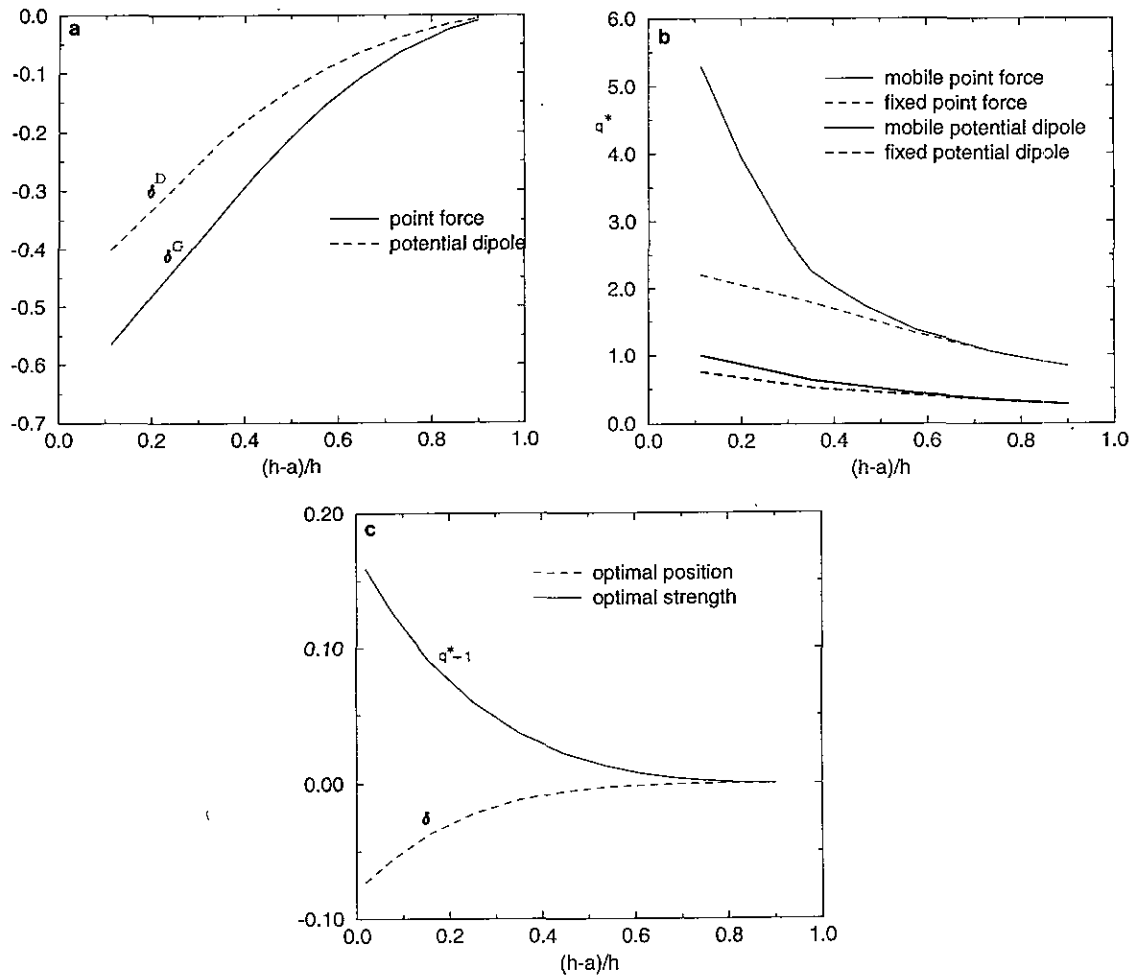

FIG. 7. A sphere translating normal to a plane wall: (a) displacement of the point force, δ^G and potential dipole δ^D off the center of the sphere; (b) associated optimal strengths q^* as functions of the sphere-to-wall separation. (c) A sphere rotating around an axis that is perpendicular to a plane wall; the displacement and optimal strength of the couplet as a function of the dimensionless sphere-to-wall separation.

towards the wall. For instance, when $h/a = 10.06766$, the displacement of the point force from the center of the sphere is less than 1% the sphere radius, but increases to more than half the sphere radius for $h/a = 1.127626$. When the singularities are placed initially at the center of the sphere, the number of necessary iterations increases from 3 to 64 as h/a is decreased from 10.06766 to 1.127626.

In Table I we present the computed values of the drag coefficient λ defined in terms of the drag force by $\mathbf{D} = 6\pi\mu\lambda a\mathbf{U}$ and compare them with the exact values provided by Brenner [24, 25] obtained from a series solution in bipolar coördinates. We observe agreement in the fifth significant figure for $h/a > 6$, in the fourth significant figure for $h/a = 3.7621957$, and in the third significant figure for $h/a = 2.35241$. As the sphere approaches the wall, the error increases from less than 1% at $h/a = 1.54308$ to 24% for $h/a = 1.127626$. Thus, using two singularities provides us with accurate results only when $h/a > 1.5$. To assess the gain in accuracy due to the adaptive computation of the position of the singularities, in Table I we also include results of a computation in which the singularities are restricted to lie at the center of the sphere and the functional is optimized only with respect to their strength. The corresponding strengths of the fixed singularities are shown in Fig. 7b. Comparisons show that the solutions with moving singularities are substantially more accurate than those for fixed singularities, especially at close sphere-to-wall separations.

Using a higher number of singularities extends the range of accuracy of the method to smaller sphere-to-wall separations. For instance, the drag coefficient computed using two point forces and two potential dipoles for $h/a = 1.127626$ is $\lambda = 9.190055$, which differs only by 0.67% from the exact value 9.2517663. These results encourage the application of the method to problems of bounded particulate flow.

In the case of a sphere spinning with angular velocity Ω around an axis that is perpendicular to the wall, we represent the flow in terms of a collection of couplets whose induced

TABLE II

Torque Coefficient λ for a Sphere Rotating Perpendicular to a Plane Wall

h/a	Present method	Exact solution
10.07049	1.000123	1.0001
6.13121	1.000544	1.0005
3.76223	1.002369	1.002
3.10752	1.004226	1.004
2.57732	1.007467	1.007
2.15100	1.013013	1.013
1.81061	1.022263	1.022
1.54297	1.037102	1.036
1.33743	1.059580	1.057
1.18554	1.090722	1.087
1.08108	1.127477	1.126
1.020096	1.158709	1.171

TABLE III

Drag Coefficients for the Force and Torque on a Sphere Translating Parallel to a Wall

	Present method		Exact solution	
h/a	Drag	Torque	Drag	Torque
10.0677	−1.059060	9.78725E-6	−1.0591	8.7744E-6
3.7622	−1.173777	5.54782E-4	−1.1738	4.2160E-4
2.3524	−1.307253	4.20546E-3	−1.3079	2.6423E-3
1.5431	−1.557402	3.03392E-2	−1.5675	1.4649E-2
1.1276	−2.025658	1.83382E-1	−2.1514	7.3718E-2
1.0453	−2.321323	3.33620E-1	−2.6475	1.4552E-1
1.005004	−2.595163	4.94225E-1	−3.7863	3.4187E-1

velocity vanishes over the wall. Using just one couplet we obtain results for the torque that are in remarkable agreement with the exact solution due to Jeffery [26] as shown in Table II. For instance, when $h/a = 1.02$, the difference in the computed value of the torque coefficient λ defined in terms of the torque by $\mathbf{T} = 8\pi\mu a^2\lambda\Omega$ and that given by Jeffery's exact solution is only 1.1%. In Fig. 7c we present the displacement $\delta = (x - h)/a$ and optimal strength $q^* = q/(\Omega a^3)$ of the couplet. As the sphere approaches the wall, the couplet moves off the center of the sphere towards the wall, but not by a substantial distance. For instance, when $h/a = 1.02$ the couplet is located at a distance $\delta = 0.073$ below the center of the sphere.

4.2. *Sphere Translating along or Rotating around an Axis Parallel to the Wall*

In this case the flow is three-dimensional but with fore-and-aft symmetry. In the case of translation, the singularity system includes a point force and a potential dipole oriented in the direction of translation, as well as a couplet oriented parallel to the wall along the y axis. In the numerical method the singularities are allowed to move in a direction perpendicular to the wall along the x axis. In Figs. 8a, b we plot the optimal position $\delta = (x - h)/a$ and strengths of the singularities $q^{G*} = q^G/(Ua)$ and $q^{D*} = q^D/(Ua^3)$, and $q^{C*} = q^C/(Ua^2)$, and in Table III we present the values of the drag coefficients for the force and torque along with the exact values computed from a solution in bipolar coordinates [27]. For $h/a \geq 2.3524$ the computed drag force coefficient agrees with that given by the exact solution in the fourth significant figure, but for lower separations we obtain significant discrepancies. The disagreement for the torque coefficient is prominent, due to the fact that its small numerical values are shielded by the dominant contributions due to numerical error.

To improve the accuracy we used a higher number of singularities but found that, during the iterations, the singularities approach each other to form dipoles. This is interpreted as

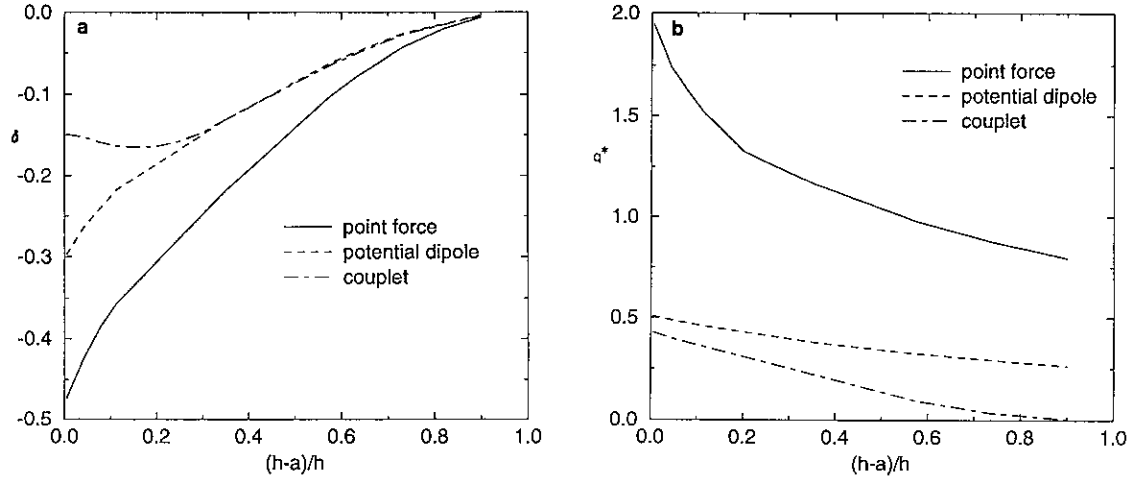

FIG. 8. A sphere translating parallel to a plane wall. (a) Displacement δ of the point force (solid line), potential dipole (dashed line), and couplet (long-dashed line), off the center of the sphere; (b) associated optimal strengths q^* as functions of the dimensionless sphere-to-wall separation.

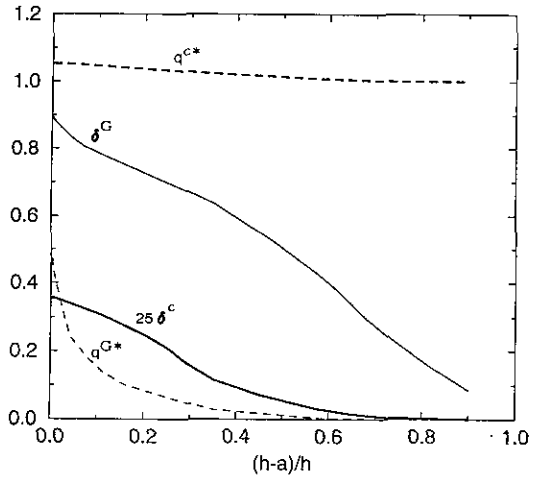

FIG. 9. A solid sphere rotating around an axis parallel to a plane wall. Displacement of the point force, δ^G (solid plain line), and couplet δ^C (solid bold line), off the center of the sphere, and the associated optimal strength of the point force, q^{G*} (dashed plain line), and couplet, q^{C*} (dashed bold line), as functions of the sphere center-to-wall separation.

TABLE IV

Force and Torque Coefficients of a Sphere Rotating Parallel to a Plane Wall

	Present method		Exact solution	
h/a	Drag	Torque	Drag	Torque
10.0677	1.03768E-5	1.000123	1.1699E-5	1.0003
3.7622	5.90360E-4	1.002417	5.6214E-4	1.0059
2.3524	4.32729E-3	1.010402	3.5231E-3	1.0250
1.5431	2.8761E-2	1.042248	1.9532E-2	1.0998
1.1276	1.38501E-1	1.153471	9.8291E-2	1.3877
1.0453	2.40875E-1	1.252447	1.9403E-1	1.6996
1.005004	4.42339E-1	1.444596	4.5582E-1	2.5056
1.003202	4.70858E-1	1.472401	5.1326E-1	2.6793

evidence that higher order singularities such as the point force dipole, potential quadruple, and couplet dipole are more appropriate in the singularity representation.

In the case of a sphere rotating around an axis that is parallel to a plane wall, the singularity system includes a point force oriented parallel to the wall but perpendicular to the axis of rotation and a couplet oriented along the axis of rotation. Both the point force and couplet are located at the center of the sphere initially and are allowed to move along the x axis throughout the computation. The optimal location and strength of the singularities are shown in Fig. 9. Comparing the computed drag coefficient for the force and torque with the exact solution in bipolar coordinates of Goldman *et al.* [27], shown in Table IV, reveals noticeable discrepancies, even at large separations. Using a higher number of singularities we run into convergence difficulties associated with the formation of dipoles, once again indicating a necessity for including higher-order singularities in the discrete representation.

4.3. *A Sphere in a Simple Shear Flow*

As a last case, we consider flow past a sphere that is held stationary in a simple shear flow $\mathbf{u}^\infty = (0, 0, kx)$, above a plane wall as shown in Fig. 6b. The singularity system involves point forces, potential dipoles, and couplets, situated and allowed to move along the x axis. The point forces and potential dipoles are oriented in the streamwise direction, whereas the couplets are oriented along the y axis. Numerical experimentation showed that the best results are achieved using two point forces, two potential dipoles, and one couplet. The optimal positions

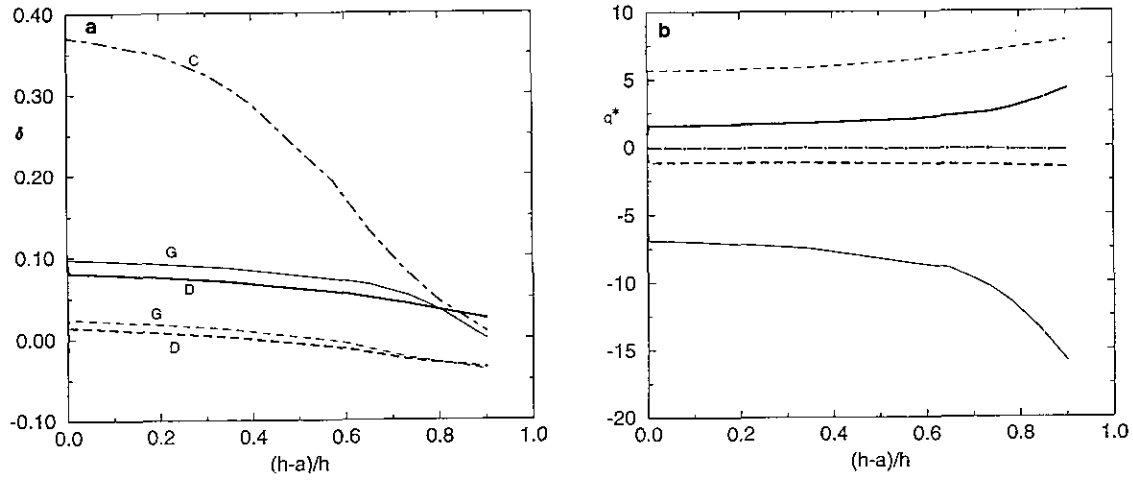

FIG. 10. A solid sphere placed in a simple shear flow above a plane wall. (a) Displacements of the point forces δ^G (plain solid and plain dashed line), potential dipoles δ^D (bold solid and bold dashed line), and couplet δ^C (dot-dashed line); (b) corresponding optimal strengths q^* as functions of the sphere-to-wall separation.

TABLE V

Force and Torque on a Stationary Sphere in a Simple Shear Flow

	Present method		Faxen's Law		Exact solution	
h/a	Drag	Torque	Drag	Torque	Drag	Torque
∞	1	1			1	1
10.0677	1.058738	0.999928	1.058737	0.999922	1.0587	0.99981
3.7622	1.167119	0.998470	1.167059	0.998117	1.1671	0.99711
2.3524	1.277894	0.993005	1.277323	0.991888	1.2780	0.99010
1.5431	1.436590	0.975395	1.434287	0.971809	1.4391	0.97419
1.1276	1.603623	0.949630	1.597015	0.949103	1.6160	0.95374
1.0453	1.650884	0.943320	1.637376	0.949619	1.6682	0.94769
1.005004	1.675926	0.940954	1.654914	0.947708	1.6969	0.94442
1.003202	1.677066	0.940878		0.947839	1.6982	0.94427
1.0000	1.679014	0.941140			1.7005	0.94399

and strengths of the singularities are plotted in Figs. 10a, b, where $q^{G*} = q^G/(ka^2)$, $q^{D*} = q^D/(ka^4)$, $q^{C*} = q^C/(ka^3)$.

The numerical results for the drag force and torque coefficients shown in Table V are compared with the exact solution in bipolar coordinates provided by Goldman *et al.* [28]. The agreement ranges from excellent to good. It is striking to observe that even when the sphere touches the wall, the error in the drag force is less than 2%, and in the torque it is less than 1%.

It is interesting to compute the force and torque exerted on the sphere using Faxen's laws, derived on the basis of the singularity representations for translation and rotation discussed previously in this section. The results computed using the generalized Faxen relations, shown in Table V, are comparable to the numerical solutions and provide us with accurate approximations to the exact solutions. In this light, the singularity locations and strengths presented in previous tables and figures acquire special significance for computing particle motions in a viscous fluid.

ACKNOWLEDGMENTS

This research is supported by the National Science Foundation, Grant CTS-9216176. Additional support is provided by the Exxon Education Foundation and the Department of Energy. The authors thank Professor G. Fairweather for providing reprints of his work on the method of fundamental solutions.

REFERENCES

1. A. T. Chwang and T. Y. Wu, *J. Fluid Mech.* **63,** 607 (1974).
2. A. T. Chwang and T. Y. Wu, *J. Fluid Mech.* **67,** 787 (1975).
3. S. Kim and P. V. Arunachalam, *J. Fluid Mech.* **178,** 535 (1987).
4. S. Kim and S. Karrila, *Microhydrodynamics: Principles and Selected Applications* (Butterworth-Heinemann, Stoneham, MA, 1991).
5. C. Pozrikidis, *Boundary Integral and Singularity Methods for Linearized Viscous Flow* (Cambridge, Univ. Press, Cambridge, UK, 1992).
6. T. Dabros, *J. Fluid Mech.* **156,** 1 (1985).
7. A. Bogomolny, *SIAM J. Numer. Anal.* **22**(4), 644 (1985).
8. R. A. Mathon and R. L. Johnson, *SIAM J. Numer. Anal.* **14**(4), 638 (1977).
9. R. L. Johnson and R. A. Mathon, *Int. J. Numer. Methods Eng.* **14,** 1739 (1979).
10. D. Redekop, *Appl. Math. Modeling* **6,** 390 (1982).
11. R. L. Johnson and G. Fairweather, *Appl. Math. Modeling* **8,** 265 (1984).
12. P. S. Han, M. D. Olson, and R. L. Johnson, *J. Eng. Comput.* **1,** 232 (1984).
13. P. S. Han and M. D. Olson, *Int. J. Numer. Methods Eng.* **24,** 1187 (1986).
14. P. S. Kondapalli, D. J. Shippy, and G. Fairweather, *Comput. Methods Appl. Mech. Eng.* **96,** 255 (1992).
16. P. S. Kondapalli, D. J. Shippy, and G. Fairweather, *J. Acoust. Soc. Am.* **91**(4), 1844 (1992).
17. A. Karageorghis and G. Fairweather, *J. Comput. Phys.* **69,** 434 (1987).
18. A. Karageorghis and G. Fairweather, *Int. J. Numer. Methods Eng.* **26,** 1665 (1988).
19. A. Karageorghis and G. Fairweather, *Int. J. Numer. Methods Fluids* **9,** 1221 (1989).
20. A. Karageorghis and G. Fairweather, *IMA J. Numer. Anal.* **9,** 231 (1989).
21. A. Karageorghis, *J. Comput. Phys.* **98,** 119 (1992).
22. G. Papanikolaou and J. Zhu, *Commun. Pure Appl. Math.* **44,** 101 (1991).
23. A. H. Stroud, *Approximate Calculation of Multiple Integrals* (Prentice-Hall, Englewood Cliffs, NJ, 1971), p. 361.
24. J. Happel and H. Brenner, *Low Reynolds Number Hydrodynamics* (Martinus Nijhoff, Dordrecht, 1983).
25. H. Brenner, *Chem. Eng. Sci.* **16,** 242 (1961).
26. G. B. Jeffery, *Proc. London Math. Soc.* **14,** 327 (1915).
27. A. J. Goldman, R. G. Cox, and H. Brenner, *Chem. Eng. Sci.* **22,** 637 (1967).
28. A. J. Goldman, R. G. Cox, and H. Brenner, *Chem. Eng. Sci.* **22,** 653 (1967).